Significant impacts of radiation physics in the Weather Research and Forecasting model on the precipitation and dynamics of the West African Monsoon

R. Li · J. Jin · S.-Y. Wang · R. R. Gillies

Abstract Precipitation from the West African Monsoon (WAM) provides food security and supports the economy in the region. As a consequence of the intrinsic complexities of the WAM's evolution, accurate simulations of the WAM and its precipitation regime, through the application of regional climate models, are challenging. We used the coupled Weather Research and Forecasting (WRF) and Community Land Model (CLM) to explore impacts of radiation physics on the precipitation and dynamics of the WAM. Our results indicate that the radiation physics schemes not only produce biases in radiation fluxes impacting radiative forcing, but more importantly, result in large bias in precipitation of the WAM. Furthermore, the different radiation schemes led to variations in the meridional gradient of surface temperature between the north that is the Sahara desert and the south Guinean coastline. Climate diagnostics indicated that the changes in the meridional gradient of surface temperature affect the position and strength of the African Easterly Jet as well as the low-level monsoonal inflow from the Gulf of Guinea. The net result was that each radiation scheme produced differences in the WAM precipitation regime both spatially and in intensity. Such considerable variances in the WAM precipitation regime and dynamics, resulting from radiation representations, likely have strong feedbacks within the climate system and so have inferences when it comes to aspects of predicted climate change both for the region and globally.

1 Introduction

In West Africa, food security and the economy rely heavily upon agricultural production that is strongly dependent on the precipitation from the West African Monsoon (WAM). The WAM of western Sub-Saharan Africa is a complex phenomenon, that is, to first order, characterized by a northward propagation of a zonally oriented precipitation field (rain-belt) that, during the summer months [June, July, and August (JJA)], moves roughly between the Gulf of Guinea and the ecoclimatic and biogeographic zone of transition referred to as the Sahel (i.e., between latitudes 9° and 20° N). The formation of the WAM is the result of seasonal shifts and interactions between (a) the Inter-Tropical Convergence Zone (ITCZ), (b) the westerly monsoonal wind flow, (c) the African Easterly Jet (AEJ), (d) the Tropic Easterly Jet (TEJ), and (e) African Easterly Waves (AEW) (Wang and Gillies 2011; Pu and Cook 2012; Nicholson et al. 1998; Druyan and Koster 1989). Additionally, several isolated plateaus and mountain ranges rise from the Sahel and interact with the rain-belt's northerly progression, further complicating its dynamics.

As a consequence of the intrinsic complexities of the WAM's evolution, accurate simulations of the WAM through the application of regional climate models (RCMs) pose a particular challenge. For example, in earlier versions

R. Li (✉) · S.-Y. Wang · R. R. Gillies
Utah Climate Center, Utah State University, Logan, UT, USA
e-mail: lirong18@gmail.com

R. Li · J. Jin · S.-Y. Wang · R. R. Gillies
Department of Plants, Soils, and Climate, Utah State University, Logan, UT, USA

J. Jin
Department of Watershed Sciences, Utah State University, Logan, UT, USA

of the RCMs [e.g., the fifth-generation Mesoscale Model (MM5)], simulations tended to yield a somewhat narrow rain-belt along with disproportionate precipitation amounts along the core in contrast to climatology (e.g., Vizy and Cook 2002). Subsequent simulations of, for example, Pal et al. (2007) who modeled the WAM for the time period 1987–2000 using the (International Centre for Theoretical Physics) Regional Climate Model version 3 (RegCM3), likewise produced an excess of precipitation but placed the rain-belt too far to the north in comparison to observations. Similar biases in the amount and placement were also produced by the Modèle Atmosphérique Régional (MAR) model (Gallee et al. 2004). In stark contrast, application of the same model as in Pal et al. (2007) (i.e., RegCM3, but with a different convection scheme (i.e., the Grell scheme), resulted in the rain-belt position being offset too far south (Afiesimama et al. 2006).

Some regional climate models make available a suite of schemes within the models' radiation (RA), microphysics (MP), cumulus (CU), planetary boundary layer (PBL), and land-surface (LS) parameterizations; these options serve as useful tools in such matters as sensitivity studies as well as which options serve to capture the meteorological conditions best. For example, Steiner et al. (2009) showed that RegCM3 simulations of the WAM were sensitive to different land-surface schemes. What is more, they also showed that the performance of the Community Land Model [(CLM), Bonan et al. 2002], a land-surface component, in capturing the precipitation and dynamics of the WAM, was superior in comparison to the Biosphere Atmosphere Transfer Scheme (BATS). A further study of Flaounas et al. (2011) conducted six simulations to test the combinations of three CU schemes and two PBL schemes embedded within the Weather Research and Forecasting (WRF) model. Flaounas et al. (2011) discovered that each combination produced noticeably differing simulations of the precipitation field, while none captured the strong rainfall regime that is observed to occur over the Cameroon Mountains (10° E, 5° N–7° N)—a distinctive topographically forced feature in the WAM precipitation field.

In general, model sensitivity studies with respect to the WAM have focused primarily on the CU, PBL and LS schemes. The studies have not only overlooked the role that the other two schemes (RA & MP) might play but perhaps, more importantly, have not considered the fact that each of the five categories might induce biases into the simulations to differing degrees. Hence, we decided to scrutinize the precipitation variance in a coupled WRF-CLM model for a given set of the five parameterization categories; the structure of the sensitivity experiments along with the results are outlined in Sects. 2 and 3 respectively. Following on from what we found from the sensitivity tests, we then examined more closely the role of the WRF-CLM RA schemes on the

WAM precipitation field and dynamics that may provide a strong feedback to the climate system—something which, to date, has not been done but was found, in this study, to be equally, if not more, important than the CU, PBL and LS schemes. The paper arrangement follows the customary format—methodology and data sources (Sect. 2), results (Sect. 3) with Sect. 4 summarizing what we found that subsequently directed our conclusions and initiated some discussion.

## 2 Methodology and data sources

2.1 Data

Several datasets were used to evaluate model performance. For gridded precipitation, we used the University of Delaware observations (UDel) (Willmott et al. 1994); this is a gauge-based dataset at 0.5° resolution. Measured surface temperatures and radiation fluxes were obtained from the National Aeronautics and Space Administration (NASA) (Darnell et al. 1988; Gupta et al. 1992; Whitlock et al. 1995). The resolution of the NASA datasets is 1.0°. For comparison of the wind fields, we used the Climate Forecast System Reanalysis dataset (CFSR; Saha et al. 2010).

2.2 Model configuration, calibration and RA simulations

We utilized the Weather Research and Forecasting model (WRF) version 3.2.1 (http://www.wrf-model.org/index.php) coupled to the Community Land Model (CLM) version 3.5 (Jin and Wen 2012; Subin et al. 2011), denoted as WRF-CLM. Initial and lateral boundary conditions were obtained from the six-hourly NCEP-NCAR reanalysis (Kalnay et al. 1996), which also provided sea surface temperatures (SST). The model domain is shown in Fig. 1; the extent of the domain was designed to cover most of the African continent and to include the eastern part of the Atlantic Ocean. The spatial resolution was set to 30 km, resulting in 221 × 141 grids. At such a resolution, topography was considered to be reasonably resolved. For land use types we utilized the United States Geological Survey (USGS) 24-category global 30-s dataset. The WRF-CLM simulations used 27 vertical layers, and the top of the atmosphere was set to 50 hPa.

Our first task was to evaluate the WAM precipitation variance simulated using the different physics schemes in WRF-CLM. The set comprised five LS, three RA combinations (i.e., long-wave & short-wave couples), four CU, four PBL, and eight MP parameterizations. In the end, 24 simulations, each comprising a different combination of these physics schemes, were computed for the precipitation biases using UDel precipitation as true. The biases were then used to calculate the variance.

Fig. 1 The WRF-CLM model domain with topography outlined in *color*. The important topographical regions are marked
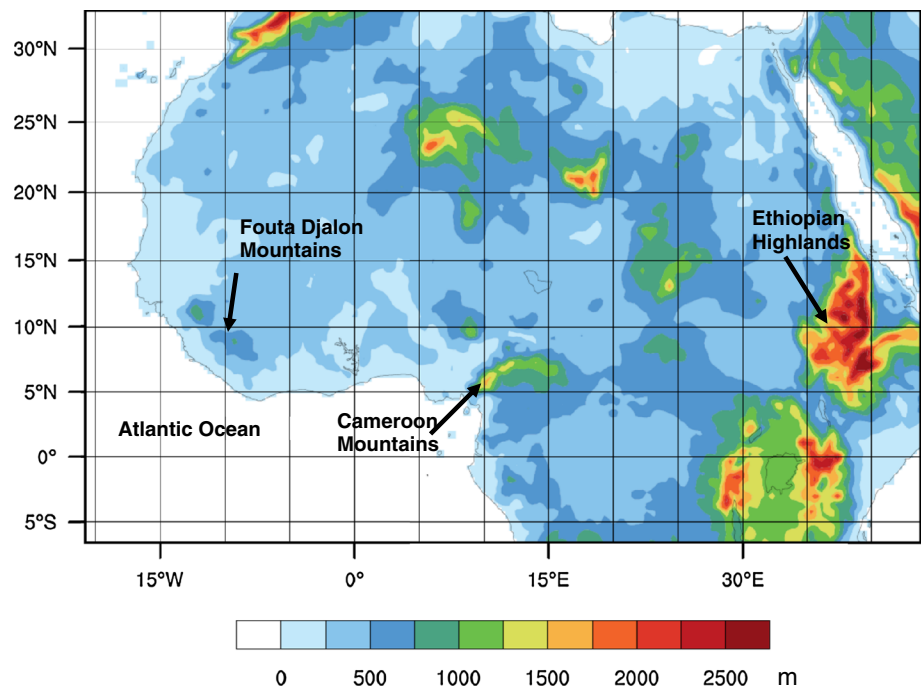
The calibration of WRF-CLM for the purpose of RA assessment began by conducting a series of sensitivity tests. Since conducting sensitivity tests over a long time period is expensive, we decided upon an approach that would identify the month and year where the monthly precipitation was closest to the WAM climatology in terms of precipitation amount and pattern; this approach is different in comparison to previous studies where the entire monsoon season (e.g., Flaounas et al. 2011) or a longer term (e.g., 10 years by Steiner et al. 2009) was used. Therefore, our first task was to create the climatology and so, we calculated, using the UDel gridded dataset, the precipitation average over the period 1981 to 2010 for the core months of the monsoon season (i.e., June, July, and August—JJA). Next, for each monsoon month (JJA) for years 1981–2010, we computed the Root Mean Square Deviation (RMSD) and the spatial correlation coefficient (R) between its monthly precipitation and the climatology precipitation average over the domain. The results indicated that the precipitation for July 2002 had the greatest R and least RMSD among all 90 months; this signified that the monthly precipitation of July 2002 was closest to the JJA climatology of 1981–2010—illustrated in Fig. 2. Our approach was designed as a balance between model optimization and computational costs, since simulating a 30-year climatology for each combination of physics schemes is cost-prohibitive.

Once the month of July 2002 was established as representative, a series of sensitivity tests were conducted for the month of July 2002 to obtain a combination of physics

schemes that produced the best WAM precipitation field; these involved 24 different parameterizations in WRF-CLM (five LS, three RA combinations, four CU, four PBL, and eight MP parameterizations). The parameterization schemes selected were the combination that yielded the least WAM precipitation bias based once again on that which had the greatest R and least RMSD; the best combination turned out to be Betts-Miller-Janjic—BMJ (CU), Lin (MP), YSU (PBL), and CLM (LS) schemes.

The simulations that were used to ascertain the role of the WRF-CLM RA schemes on the WAM precipitation field were conducted using the following three combinations of long-wave (LW) and short-wave (SW) radiation schemes: (a) RRTM (the Rapid Radiative Transfer Model)—Dudhia (referred to as R1), (b) CAM (Community Atmosphere Model)—CAM (R2), and (c) RRTMG-RRTMG (R3); the details are listed in Table 1. In doing so, we used the selected combination of physics schemes and, this time around, simulated the WAM precipitation fields for May through August 2002. The month of May 2002 simulations were treated as spin-up and were excluded from the analysis.

3 Results

3.1 Precipitation

The range of precipitation variance simulated using the different physics schemes in WRF-CLM, including five LS,

Fig. 2 Monthly precipitation in July 2002 (*upper panel*) and climatology (*lower panel*) between 1981 and 2010 from the University of Delaware observations (UDel) (Willmott et al. 1994)

UDelaware: July 2002 — mm/month

UDelaware: JJA Mean (1981-2010) — mm/month
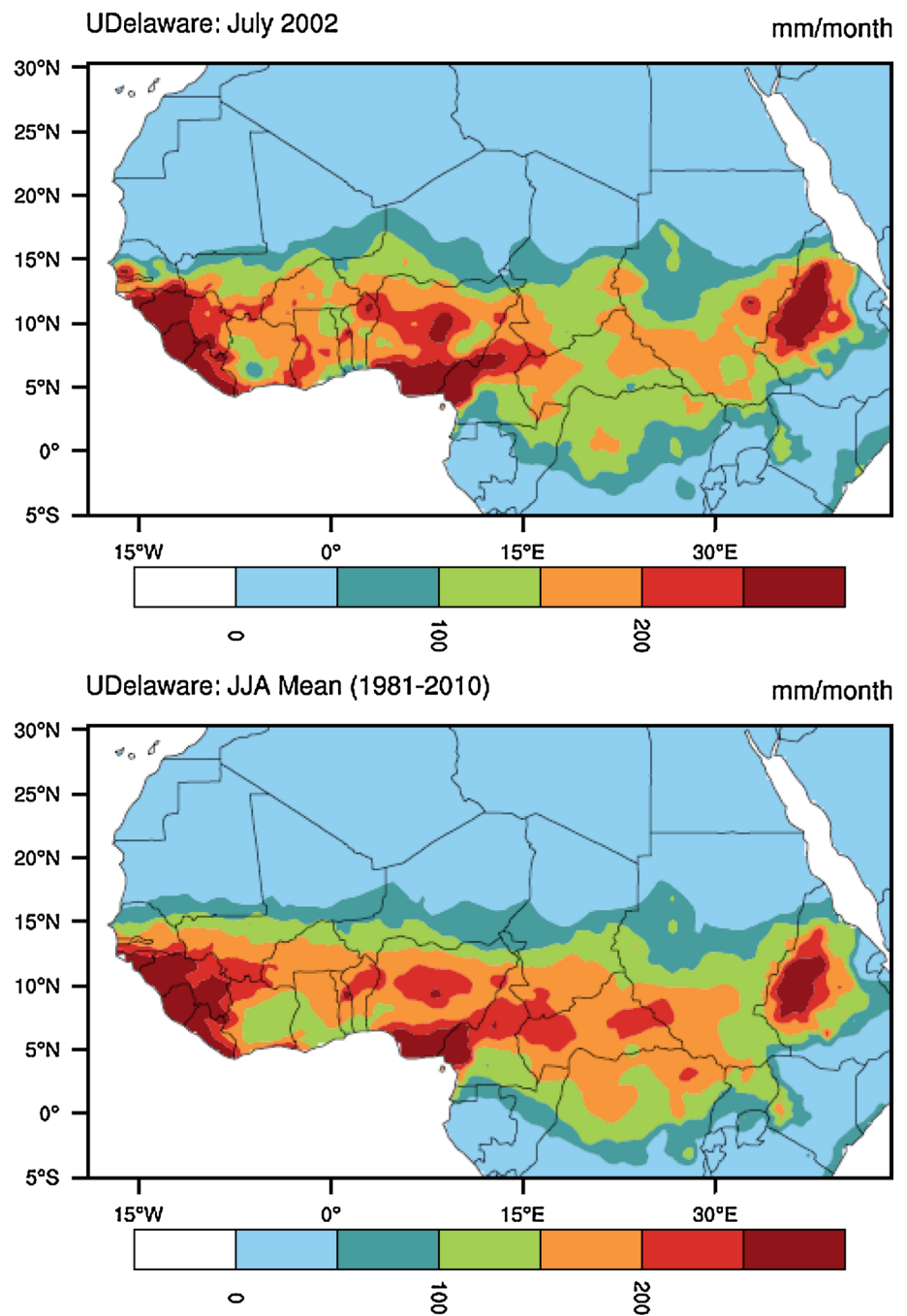
Table 1 Summary of radiation (RA) schemes tested in this study

| Simulation	Wavelengths	Schemes	Major characteristics
R1	LW	RRTM (Clough et al. 2005; Mlawer et al. 1997)	K-distribution method with 256 g points
	SW	Dudhia (Dudhia 1989)	Calculation of clear-air scattering, water vapour absorption, and cloud albedo and absorption using look-up tables for clouds from Stephens (1978)
R2	LW	CAM (Collins et al. 2006)	Absorptivity/emissivity formulation methods based on Ramanathan and Downey (1986)
	SW	CAM (Collins et al. 2006)	Delta-Eddington approximation method
R3	LW	RRTMG (Clough et al. 2005)	K-distribution method with 140 g points
	SW	RRTMG (Clough et al. 2005)	K-distribution method with 112 g points
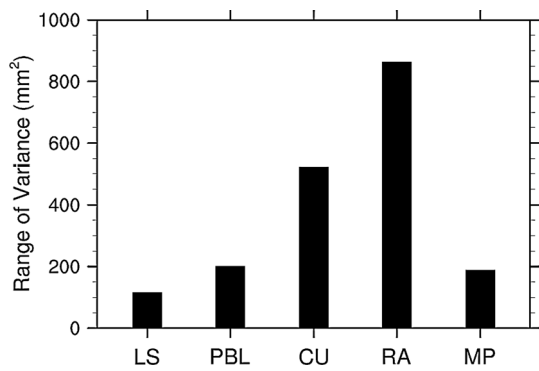
Fig. 3 Range of precipitation variance for the tested land surface (LS), planetary boundary layer (PBL), cumulus convection (CU), radiation (RA), and microphysics (MP) schemes

three RA combinations, four CU, four PBL, and eight MP parameterizations is summarized Fig. 3. It is noted that the maximum range of precipitation variance (i.e., biases) appears in the radiation scheme simulations, having outweighed those resulting from any other scheme categories. This result is surprising and has a strong implication on

the simulation of the WAM, as previous research almost always focused on CU, PBL, or LS processes but apparently had overlooked the effect of radiative processes.

The observed and simulated monthly rainfall averaged over June through August 2002 is shown in Fig. 4. The typical zonal rain-belt of the WAM is revealed in the observations (Fig. 4a) that lies between the equator and 18°N; this is associated with the AEJ and low-level monsoonal flow (Cook 1999). Three locations of maximum rainfall are apparent: (a) over the Fouta Djalon Mountains, (b) the Cameroon Mountains, and (c) the Ethiopian Highlands.

The precipitation in the R1 simulation (Fig. 4b) conforms well with the observations both spatially and in magnitude. More specifically, the WRF-CLM simulation captured both the northern latitudinal position and extent of the rain-belt as well as the maximum rainfall locations over the three aforementioned mountain regions. A quantitative assessment, by computing the spatial correlation coefficient (R), Root Mean Square Deviation (RMSD), and bias between the R1 simulation and the observations, is given in Table 2. Figure 4c presents the modeled precipitation for the R2 simulation. In comparison to the
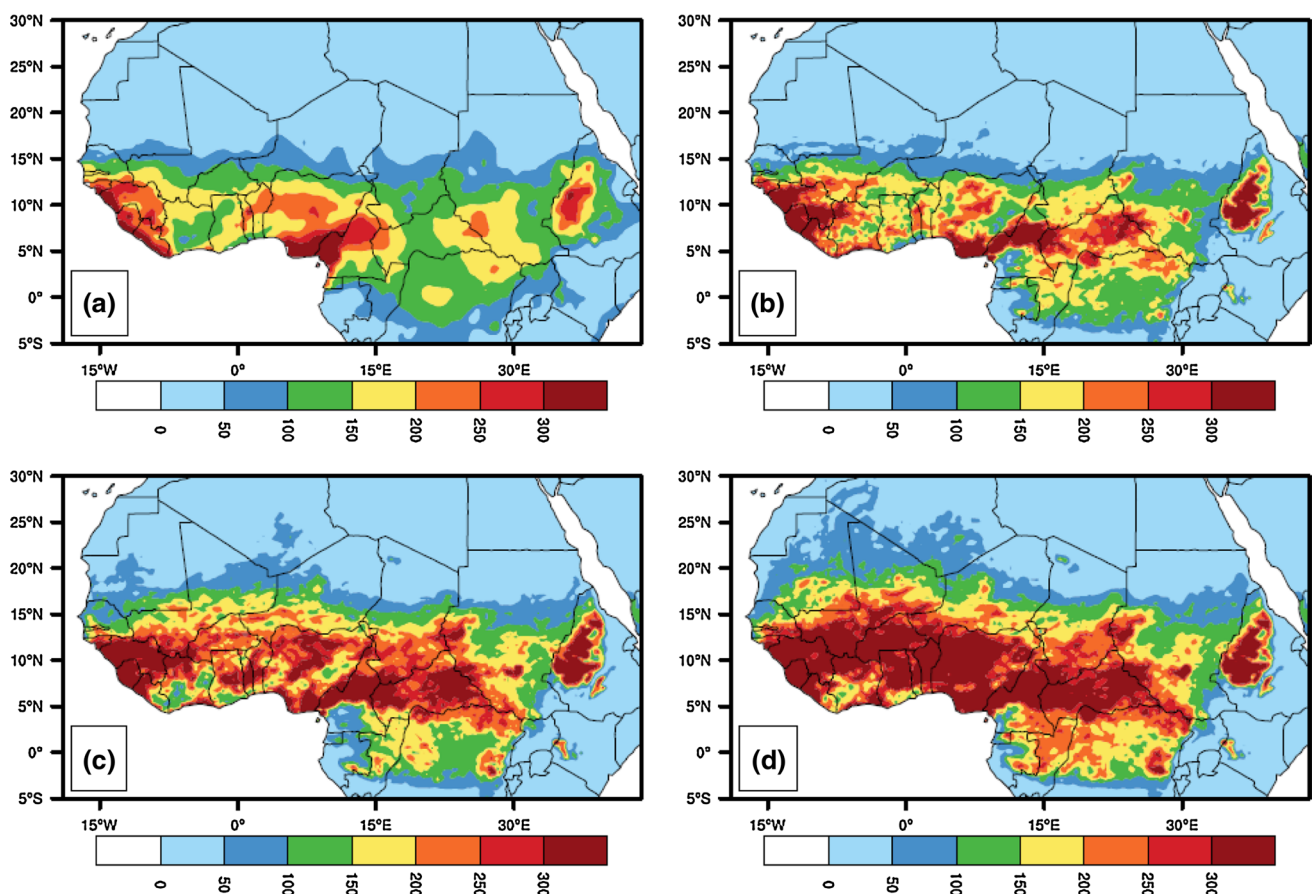
Fig. 4 Monthly precipitation (mm month^{-1}) averaged over June through August 2002 for **a** the University of Delaware observations as well as the **b** R1, **c** R2, and **d** R3 simulations

Table 2 The spatial correlation coefficient (R), root mean square deviation (RMSD), and bias between the observed and modeled precipitation

| Simulation	R	RMSD (mm/month)	Bias (mm/month)
R1	0.85	65.4	6.5
R2	0.82	93.6	36.7
R3	0.82	127.8	65.3

observations, the R2 simulation generated excessive precipitation with the rain-belt expanded too far north, beyond 20°N. Consequently, the bias of the R2 simulation is 5.6 times larger than R1 and the RMSD has increased by about 43 % (Table 2). Figure 4d displays the simulated precipitation from the R3 simulation. A similar picture to the R2 simulation is evident, but the precipitation is considerably overestimated in both latitudinal extent and amount; it even suggests rainfall within the Sahara desert. Such visible precipitation anomalies are consistent with the statistics (Table 2) showing marked bias and RMSD much larger than those in the R2 simulation.

3.2 Possible sources of precipitation differences

3.2.1 Temperature

The next step in the analysis was to examine the possible sources that led to the significant differences in precipitation between the three simulations: Fig. 5 presents (a) NASA measurements of surface temperature along with WRF-CLM simulated surface temperatures for the R1 (b), R2 (c) and R3 (d) simulations. It appears that all three simulations captured the essence of the surface temperature field in the core monsoon months along with the prominent temperature gradient between the north that is the Sahara desert and the south Guinean coastline. By comparison, the R1 surface temperature simulation is in better agreement with the observations as indicated by the statistics in Table 3 showing the lowest RMSD and highest R.

Because the north–south temperature gradient significantly affects the intensity and position of the WAM rainbelt (Cook 1999), we investigated the meridional gradients of the surface temperature fields; these are displayed in Fig. 6. Figure 6b shows that the R1 simulation realistically
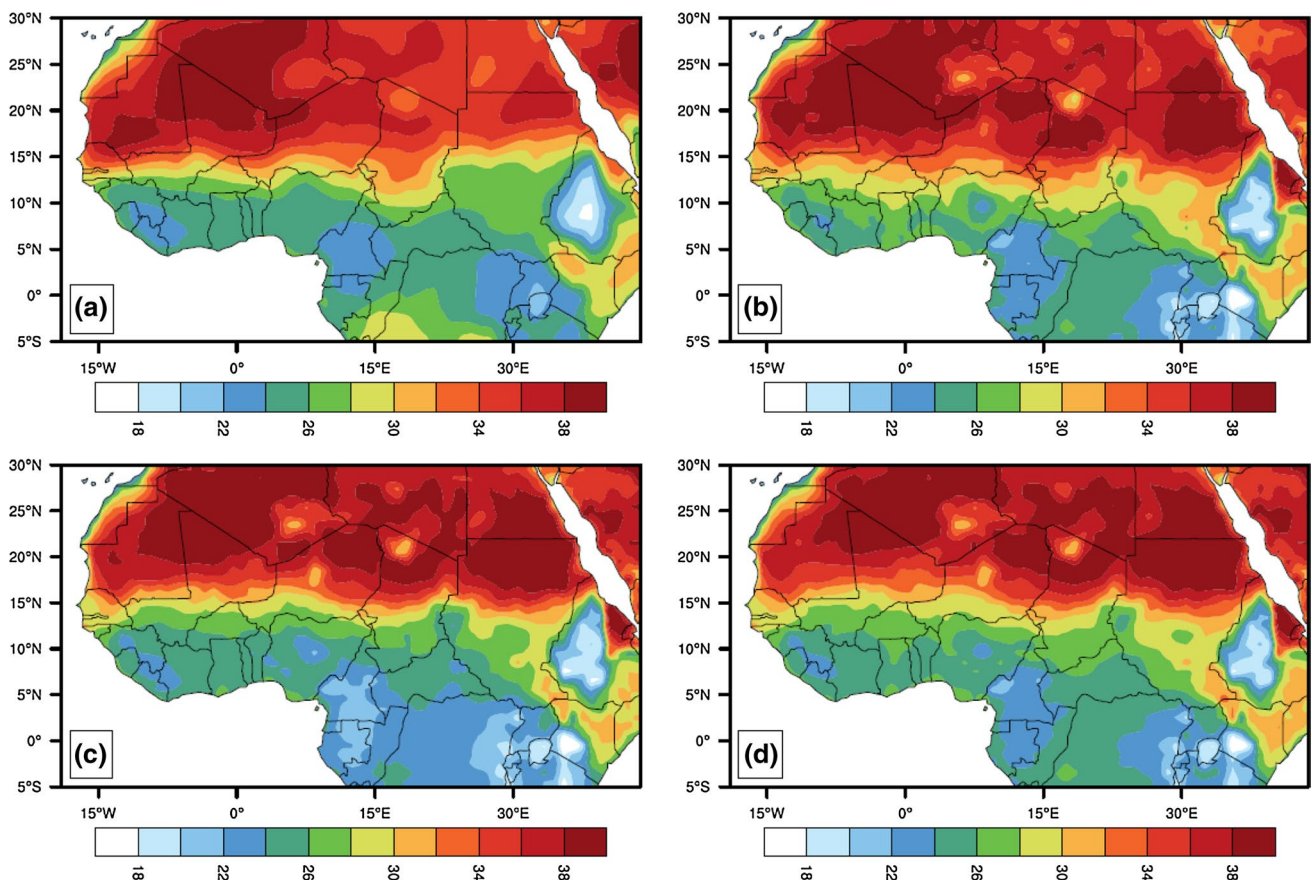
Fig. 5 Monthly surface temperature (°C) averaged over June through August 2002 for **a** the NASA observations as well as the **b** R1, **c** R2, and **d** R3 simulations

Table 3 The spatial correlation coefficient (R) and root mean square deviation (RMSD) between the observed and modeled surface temperatures

| Simulation	R	RMSD (mm/month)
R1	0.94	2.06
R2	0.94	2.26
R3	0.93	2.25

produced the meridional gradient of surface temperature when compared to the observation (Fig. 6a). Despite the difference in spatial details resulting from differences in resolutions between the observation and simulations, R1 simulated the observed band of maximum gradients along the Sahel region, peaking around 15°N. In contrast, both the R2 (Fig. 6c) and R3 (Fig. 6d) simulations shifted the band of the maximum surface temperature gradients further north into the Sahara desert, approaching 20°N. Such a degree in the shift along with an expansion of the meridional surface temperature gradient is likely to lead to

modification in atmospheric circulations and so influence precipitation; this is discussed further in Sect. 3.2.3.

3.2.2 Radiation fluxes

Since the only difference in model configuration between the three simulations is the use of different RA schemes, the differences in meridional surface temperature gradients could only have been generated by the radiation schemes. Therefore, we compared NASA's observed with simulated downward long-wave and short-wave radiation fluxes. The statistics of comparisons (ref., Table 4) indicate distinct differences: Overall, the R1 simulation achieved the highest R and lowest RMSD values for both downward long-wave and short-wave radiation fluxes, supporting the previous results in the simulation (i.e., those in Figs. 5, 6) and so, represents the most realistic simulation.

The differences in downward radiation fluxes arise because of changes in physical and numerical representations of radiative processes in the radiation schemes. It is not necessary to go into the details here but suffice it to say
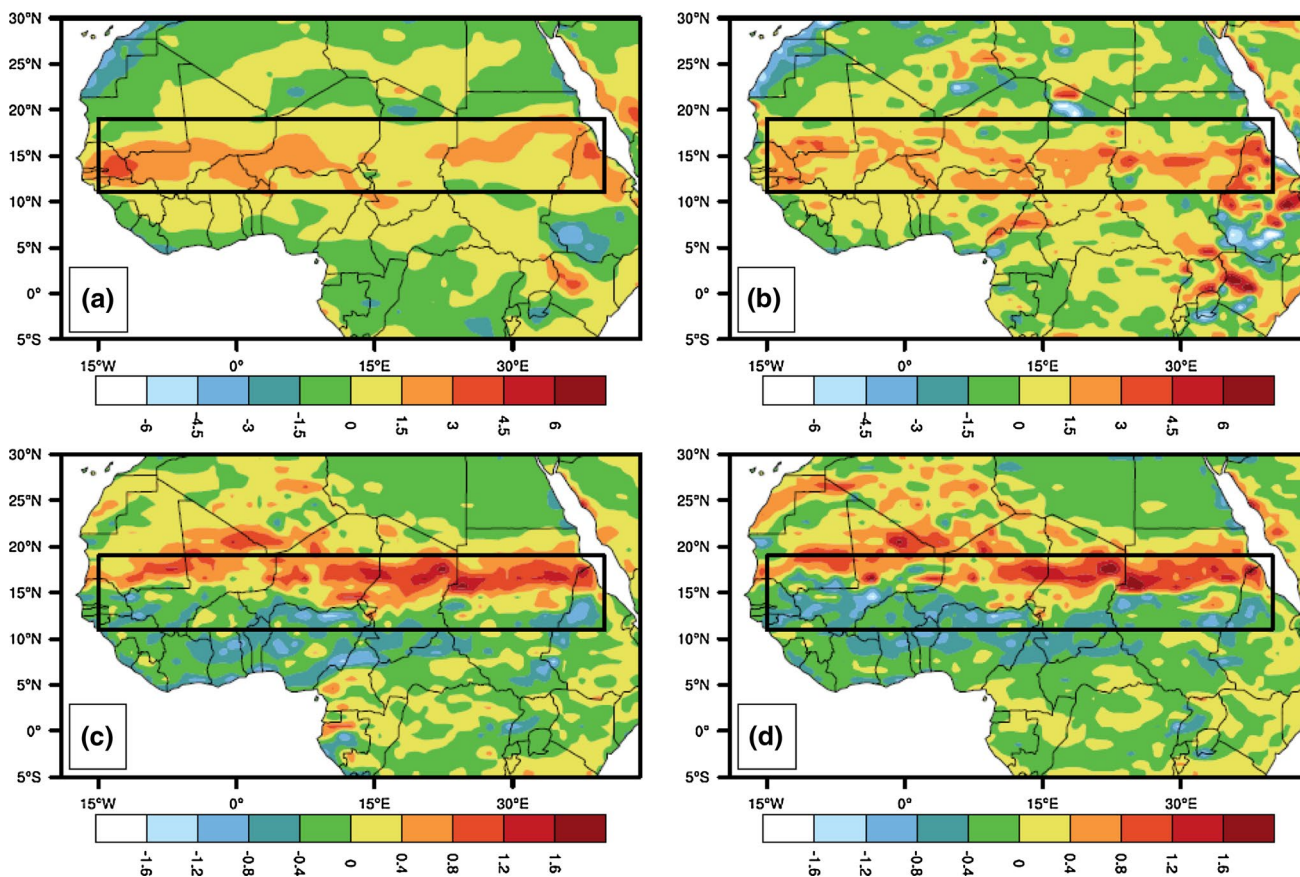
Fig. 6 The meridional gradients of surface temperature (°C/100 km) averaged over June through August 2002 with a nine-point smoothing for **a** NASA observations, **b** R1 simulation, **c** difference in surface temperature gradient between R2 and R1 simulations, and **d** difference in surface temperature gradient between R3 and R1 simulations. The *box* delineates the Sahel region

Table 4 The spatial correlation coefficient (R) and root mean square deviation (RMSD) between the observed and modeled radiation fluxes

| Wavelength	Statistics	R1	R2	R3
LW	R	0.85	0.63	0.79
	RMSD (mm/month)	13.8	21.2	14.7
SW	R	0.72	0.68	0.70
	RMSD (mm/month)	47.8	56.9	49.1

that the results of our study are similar to those published by Iacono et al. (2005).

To further illustrate how downward radiation fluxes affect the meridional gradient of surface temperature, we delineated two regions—one in the Saharan desert and the other further south within the vicinity of the Guinean coastline (ref., Fig. 7). The average temperature difference between these two regions, a representation of the north–south temperature gradient, is 9.08 °C in the R1 simulation; this coincides with the NASA observed value of 9.86 °C. However, the surface temperature differences

were over-predicted by both the R2 (12.38 °C) and R3 (11.26 °C) simulations. Moreover, we found that in the northern region, for both the R2 and R3 simulations, a positive bias in downward radiative forcings (LW + SW) was the case on the order of 26.4 and 20.8 Wm^{-2} respectively; these biases resulted in higher simulated temperatures. Contrary to the situation in the north, in the southern region both the R2 and R3 simulations exhibited a negative bias in downward radiative forcing (-26.90 and -16.40 Wm^{-2}, respectively), resulting in lower simulated temperatures. The net result is that in both cases, the meridional temperature gradient became intensified and was shifted.

### 3.2.3 Effects on the AEJ

The differences in meridional temperature gradients ultimately lead to changes in major circulation features such as the AEJ; hence, the 600-hPa observational and simulated winds are plotted in Fig. 8. The AEJ is plainly present in all three simulations. However, in comparison to the CSFR reanalysis, the R2 and R3 simulations have the jet
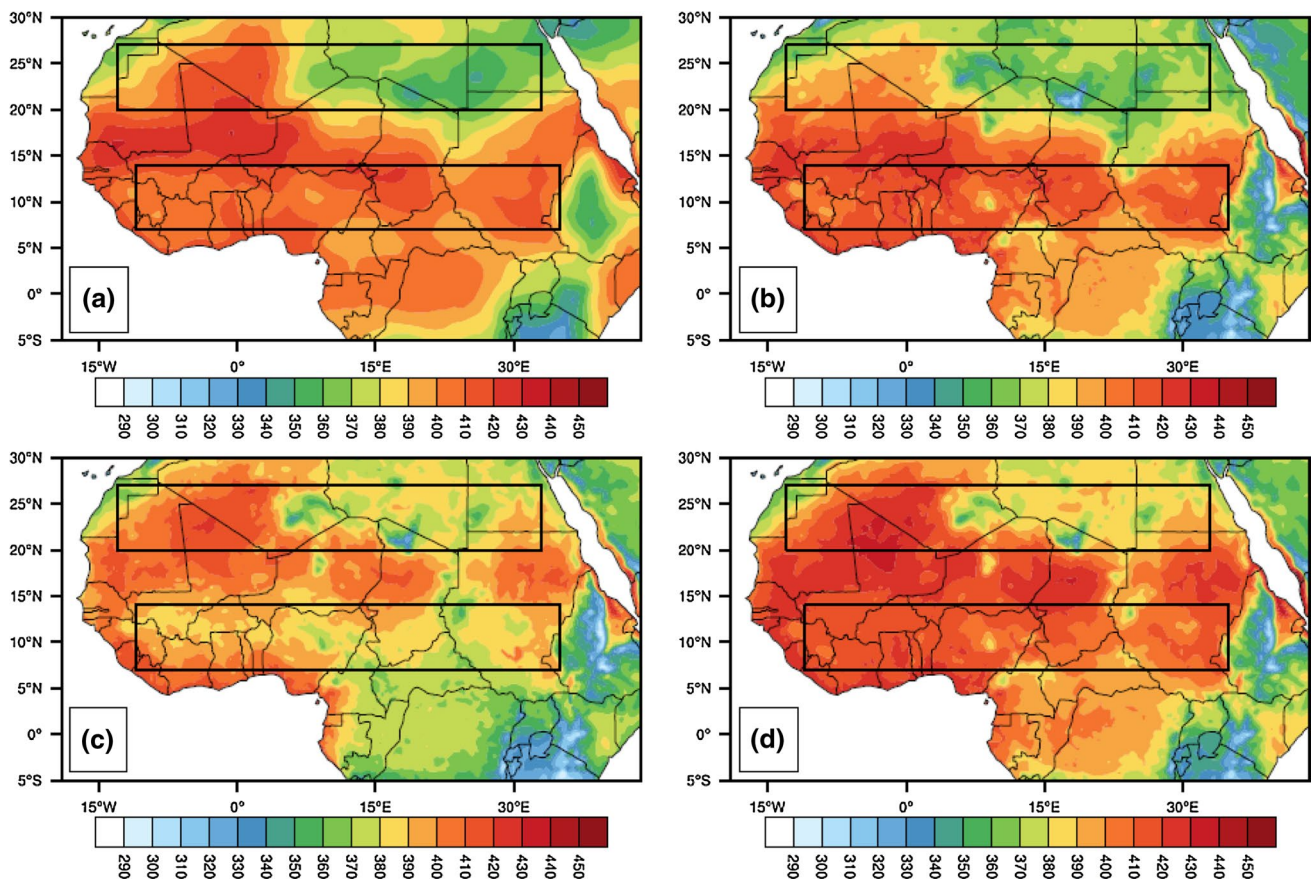
Fig. 7 Downward long-wave radiation fluxes (Wm^{-2}) averaged over June through August 2002 for **a** the NASA observations as well as the **b** R1, **c** R2, and **d** R3 simulations. The *two boxes* delineate two regions—one in the Saharan desert and the other within the vicinity of the Guinean coastline
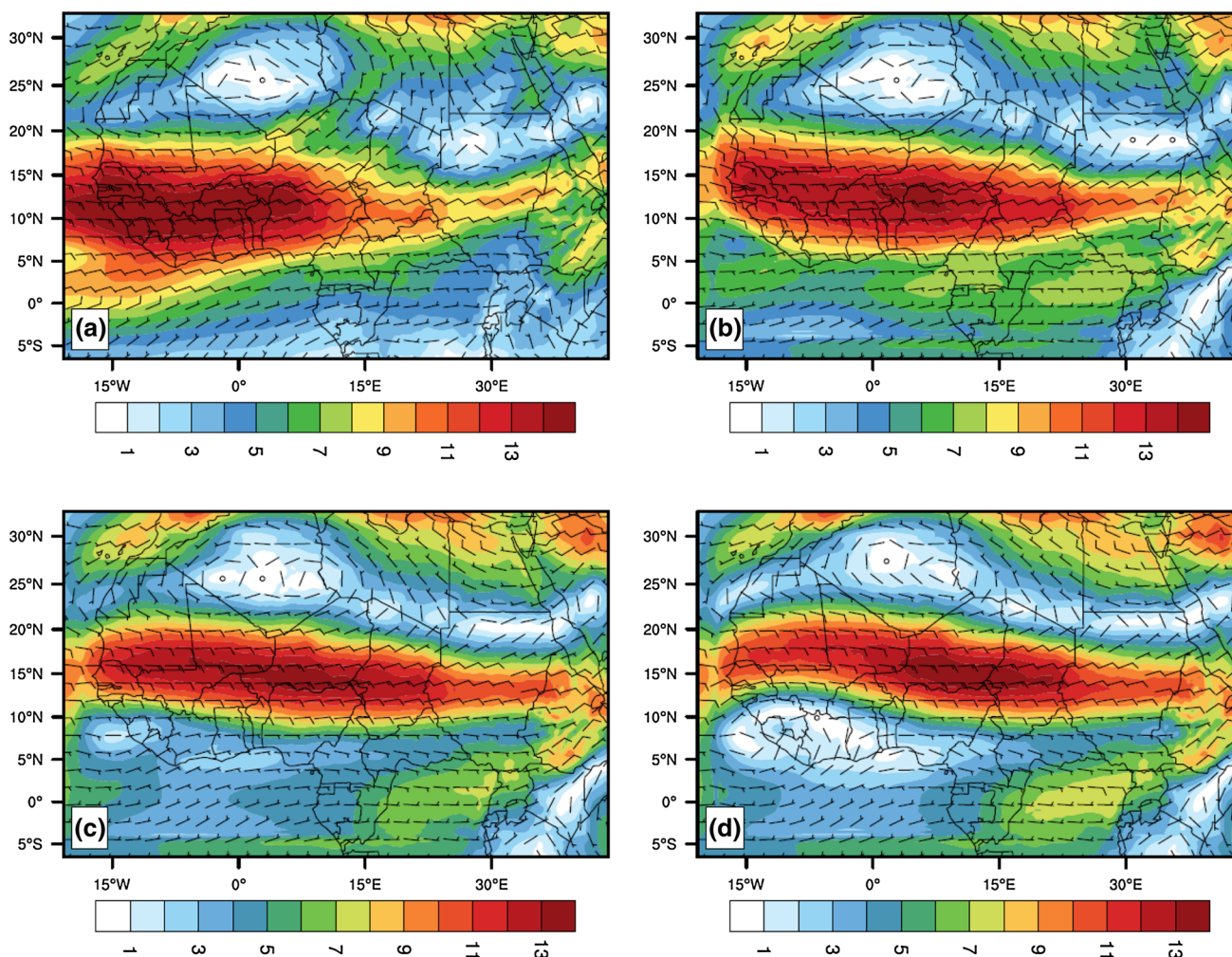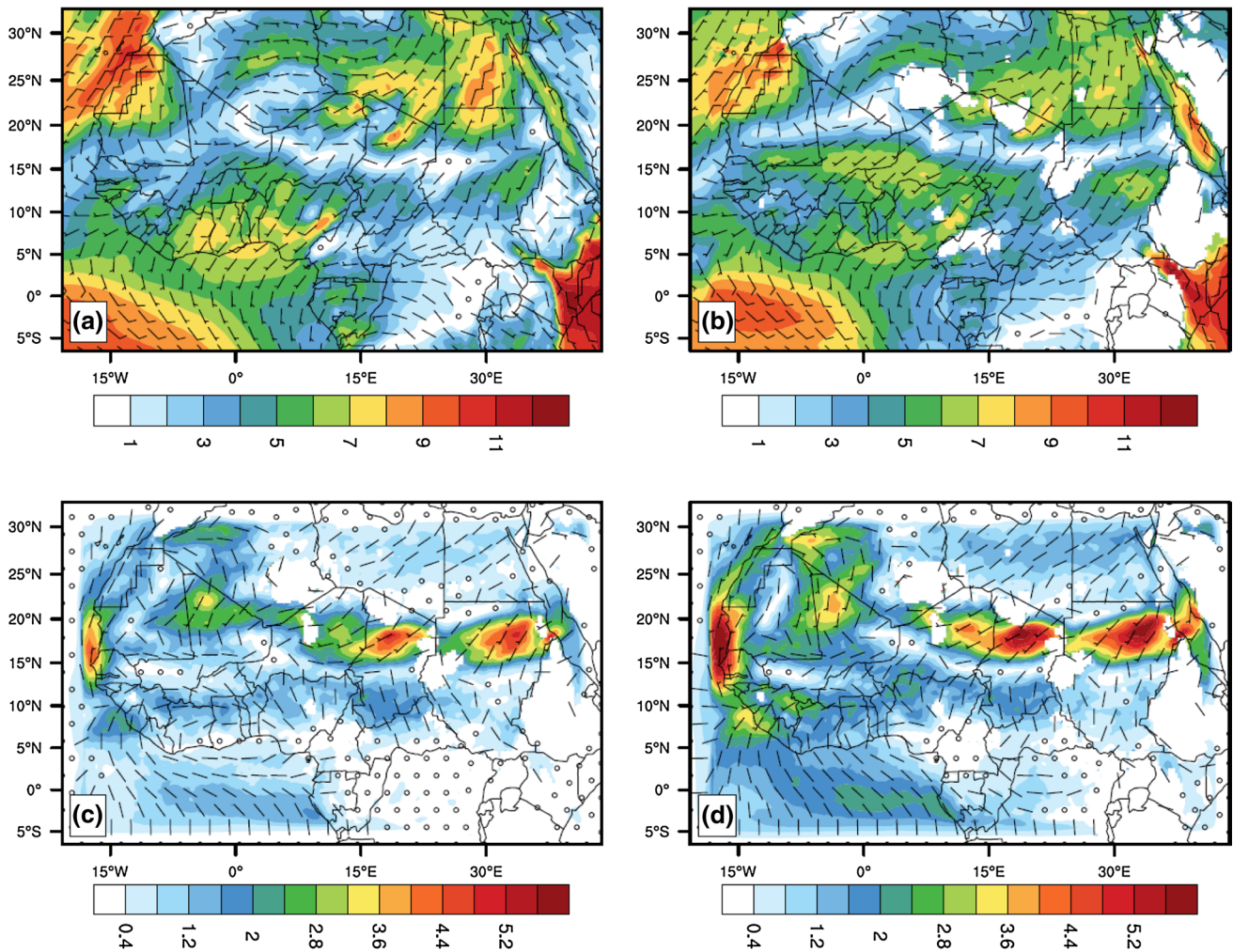
Fig. 8 Wind fields at 600 hPa (ms^{-1}) averaged over June through August 2002 for **a** the CFSR reanalysis as well as the **b** R1, **c** R2, and **d** R3 simulations

displaced somewhat northward and its latitudinal extent is narrowed, and they have it weakened over the western African coast. Given the documented close association between the changes in the Sahel rain-belt and the AEJ (e.g., Wang and Gillies 2011; Cook 1999), the bias in the R2 and R3 simulations of the extended rain-belt to the north might be induced by this northward shift of the AEJ. By comparison, the R1 AEJ characteristics are more closely aligned with the CFSR reanalysis and this is reflected in the close association between the R1-simulated and observed precipitation (ref., Fig. 4).

It has been shown that the AEJ is maintained by two diabatically forced meridional circulations: One via the surface fluxes and dry convection in the Sahara desert and the other, by deep moist convective zone equatorward of the jet (Chou and Neelin 2003; Thorncroft and Blackburn 1999). What is subsequently impacted is the activity of African Easterly Waves (AEWs) generated from the fastest-growing

linear normal mode of the summertime basic-state flow, i.e. the AEJ (Kiladis et al. 2006). About 90 % of rainfall along the Sahel region is generated by organized convective systems that are frequently initiated by AEWs (Mathon et al. 2002). Wang and Gillies (2011) also found that, since 1979, the northward shift of the Sahel rain-belt (aka, the Sahel greening) occurred in close association with the northward shift of the AEJ. Such dynamics appear to be well simulated in WRF-CLM as the bias in the AEJ from the R2 and R3 simulations (Fig. 8c, d) are consistent with the biases in the meridional temperature gradient (Fig. 6c, d) and the precipitation (Fig. 4c, d).

A further factor, to complete our examination, was a comparison of the low-level monsoonal flows between observations and the simulations (ref., Fig. 9); the comparison confirms that the R1 simulation reproduced the general features of the 925-hPa winds. However, the R3 simulation shifted the convergence zone northward and increased the strength of the

Fig. 9 Wind fields at 925 hPa (ms^{-1}) averaged over June through August 2002 for **a** CFSR reanalysis, **b** R1, **c** R2–R1, and **d** R3–R1

monsoonal inflow. A comparable effect was produced by the R2 simulation with the exception that there was a diminished strengthening of the low-level monsoonal flow while the northward shift of the convergence zone was not displaced as far. The stronger monsoonal inflow seemingly transports moisture further inland and, in combination with the northward shift of the convergence zone, contributes to enhanced precipitation. Noteworthy, however, is the consistent latitudinal position (~15°N) between the shifted convergence zone (Fig. 9c, d) and the excessive rainfall into the Sahara desert (Fig. 4c, d). What is more, is the fact that these dynamical and thermo-dynamical biases in the simulations were solely created by a change in the radiation schemes alone.

4 Summary and conclusions

While previous model sensitivity studies of the WAM primarily focused on testing CU, PBL, and LS schemes to simulate

the precipitation regime, we analyzed the impacts of radiation physics schemes on the precipitation and found that they can generate greater precipitation biases in comparison to the other physics schemes that we tested. This led to an examination of three viable scheme combinations of long-wave and short-wave in the WRF-CLM model. The simulations from the three scheme combinations (i.e., R1, R2 & R3) were compared to relevant observations. The R1 simulated the WAM precipitation field in overall agreement with observations in magnitude and placement, while the other two significantly over-predicted the precipitation field, positioning the rain-belt too far northward (into the Sahara desert). In order to appreciate the underlying mechanisms that lead to such a widespread result in precipitation, a series of climate diagnostic tests were undertaken: First, differences in the representation of radiative processes in the radiation schemes led to changes in the downward radiation fluxes; this resulted in considerable contrast in the meridional temperature gradients. These contrasts, in turn, gave rise to modifications in the monsoon

thermodynamics that produce the African Easterly Jet which, in turn, induce African Easterly Waves, as well as the dynamical processes that shape the low-level monsoonal flow, ultimately leading to the marked precipitation biases.

The best combination of physics schemes (i.e., BMJ (CU), Lin (MP), YSU (PBL), CLM (LS) and R1 (RA) schemes) identified in this study has been used to carry out a 30-year simulation of the WAM for years 1981–2010, and the simulated results have been found to be in good agreement with the observed climatology and evolution of the WAM (Li et al., in preparation). This suggests that the method described in this study, performing sensitivity tests for a deliberately selected month instead of 10 years (Steiner et al. 2009) or an entire monsoon season (Flaounas et al. 2011), is effective for identifying a representative combination of physics schemes.

A major component of global climate change is the result of the radiative forcing. In climate simulations, this forcing is determined by the radiation schemes employed. Given the relatively small value of total radiative forcing ($+2.64$ Wm^{-2}), i.e. the result of long-lived greenhouse gases (Solomon et al. 2007), accurate representation of radiative processes in climate models is essential to predicting the effects of climate change—especially so in the case of precipitation. In this study we showed that the use of different RA schemes can lead to, not only differences in radiation fluxes but more importantly, significant disparities in surface temperature fields and gradients, leading to disparities in the WAM precipitation regime both spatially and in intensity. Likewise the dynamics of the WAM was considerably influenced. The significant variances in the WAM precipitation regime and dynamics have strong feedbacks within the climate system and so, have inferences when it comes to aspects of predicted climate change for the region. The RA schemes tested in this study are used in many global and regional climate and weather models such as Community Atmosphere Model (CAM5), Community Earth System Model (CESM), WRF, MM5, and ECHAM5 (fifth-generation European Centre Hamburg Model developed at the Max Planck Institute for Meteorology), all of which are state-of-the-art climate models (Iacono et al. 2000, 2008; Morcrette et al. 2008a, b; Wild and Cechet 2002). Therefore, the predominant precipitation biases resulting from the different representations of radiation processes deserve attention.

References

Afiesimama EA, Pal JS, Abiodun BJ, Gutowski WJ Jr, Adedoyin A (2006) Simulation of West African monsoon using the RegCM3. Part I: model validation and interannual variability. Theor Appl Climatol 86:23–37

Bonan GB, Oleson KW, Vertenstein M, Levis S, Zeng XB, Dai YJ, Dickinson RE, Yang ZL (2002) The land surface climatology of the community land model coupled to the NCAR community climate model. J Clim 15:3123–3149

Chou C, Neelin JD (2003) Mechanisms limiting the northward extent of the northern summer monsoons over North America, Asia, and Africa. J Clim 16:406–425

Clough SA, Shephard MW, Mlawer E, Delamere JS, Iacono M, Cady-Pereira K, Boukabara S, Brown PD (2005) Atmospheric radiative transfer modeling: a summary of the AER codes. J Quant Spectrosc Radiat Transfer 91:233–244

Collins WD et al (2006) The formulation and atmospheric simulation of the Community Atmosphere Model version 3 (CAM3). J Clim 19:2144–2161

Cook KH (1999) Generation of the African easterly jet and its role in determining West African precipitation. J Clim 12:1165–1184

Darnell WL, Staylor WF, Gupta SK, Denn FM (1988) Estimation of surface insolation using sun-synchronous satellite data. J Clim 1:820–835

Druyan LM, Koster RD (1989) Sources of sahel precipitation for simulated drought and rainy seasons. J Clim 2:1438–1446

Dudhia J (1989) Numerical study of convection observed during the winter monsoon experiment using a mesoscale two-dimensional model. J Atmos Sci 46:3077–3107

Flaounas E, Bastin S, Janicot S (2011) Regional climate modelling of the 2006 West African monsoon: sensitivity to convection and planetary boundary layer parameterisation using WRF. Clim Dyn 36:1083–1105

Gallee H et al (2004) A high-resolution simulation of a West African rainy season using a regional climate model. J Geophys Res Atmos 109:D05108

Gupta SK, Darnell WL, Wilber AC (1992) A parameterization for longwave surface radiation from satellite data—recent improvements. J Appl Meteorol 31:1361–1367

Iacono MJ, Mlawer EJ, Clough SA, Morcrette JJ (2000) Impact of an improved longwave radiation model, RRTM, on the energy budget and thermodynamic properties of the NCAR community climate model, CCM3. J Geophys Res Atmos 105:14873–14890

Iacono MJ, Mlawer EJ, Delamere JS, Clough SA, Morcrette J, Hou Y (2005) Application of the shortwave radiative transfer model, RRTMG_SW, to the National Center for Atmospheric Research and National Centers for Environmental Prediction General Circulation Models. In: Fifteenth ARM science team meeting proceedings, Daytona Beach, FL, March 14–18, 2005

Iacono MJ, Delamere JS, Mlawer EJ, Shephard MW, Clough SA, Collins WD (2008) Radiative forcing by long-lived greenhouse gases: calculations with the AER radiative transfer models. J Geophys Res Atmos 113:D13103

Jin J, Wen L (2012) Evaluation of snowmelt simulation in the Weather Research and Forecasting model. J Geophys Res Atmos 117:D10110

Kalnay E et al (1996) The NCEP/NCAR 40-year reanalysis project. Bull Am Meteorol Soc 77:437–471

Kiladis GN, Thorncroft CD, Hall NMJ (2006) Three-dimensional structure and dynamics of African easterly waves. Part I: observations. J Atmos Sci 63:2212–2230

Mathon V, Laurent H, Lebel T (2002) Mesoscale convective system rainfall in the Sahel. J Appl Meteorol 41:1081–1092

Mlawer E, Taubman S, Brown P, Iacono M, Clough S (1997) Radiative transfer for inhomogeneous atmospheres: RRTM, a validated correlated-k model for the longwave. J Geophys Res Atmos 102:16663–16682

Morcrette J, Barker HW, Cole JNS, Iacono MJ, Pincus R (2008a) Impact of a new radiation package, McRad, in the ECMWF integrated forecasting system. Mon Weather Rev 136:4773–4798

Morcrette J, Mozdzynski G, Leutbecher M (2008b) A reduced radiation grid for the ECMWF integrated forecasting system. Mon Weather Rev 136:4760–4772

Nicholson SE, Tucker CJ, Ba MB (1998) Desertification, drought, and surface vegetation: an example from the West African Sahel. Bull Am Meteorol Soc 79:815–829

Pal JS et al (2007) Regional climate modeling for the developing world—the ICTP RegCM3 and RegCNET. Bull Am Meteorol Soc 88:1395–1409

Pu B, Cook KH (2012) Role of the West African westerly jet in Sahel rainfall variations. J Clim 25:2880–2896

Ramanathan V, Downey P (1986) A nonisothermal emissivity and absorptivity formulation for water-vapor. J Geophys Res-Atmos 91:8649–8666

Saha S et al (2010) The NCEP climate forecast system reanalysis. Bull Am Meteorol Soc 91:1015–1057

Solomon S et al (2007) Technical summary. In: Solomon S et al (eds) Climate change 2007 the physical science basis—contribution of working group I to the fourth assessment report of the intergovernmental panel on climate change. Cambridge University Press, Cambridge

Steiner AL, Pal JS, Rauscher SA, Bell JL, Diffenbaugh NS, Boone A, Sloan LC, Giorgi F (2009) Land surface coupling in regional climate simulations of the West African monsoon. Clim Dyn 33:869–892

Stephens GL (1978) Radiation profiles in extended water clouds. 2. Parameterization schemes. J Atmos Sci 35:2123–2132

Subin ZM, Riley WJ, Jin J, Christianson DS, Torn MS, Kueppers LM (2011) Ecosystem Feedbacks to climate change in california: development, testing, and analysis using a coupled regional atmosphere and land surface model (WRF3-CLM3.5). Earth Interact 15:1–38. doi:10.1175/2010EI331.1

Thorncroft CD, Blackburn M (1999) Maintenance of the African easterly jet. Q J R Meteorol Soc 125:763–786

Vizy EK, Cook KH (2002) Development and application of a mesoscale climate model for the tropics: influence of sea surface temperature anomalies on the West African monsoon. J Geophys Res Atmos 107:4023

Wang SY, Gillies RR (2011) Observed change in Sahel rainfall, circulations, African easterly waves, and Atlantic hurricanes since 1979. Int J Geophys 259529

Whitlock CH et al (1995) First global WCRP shortwave surface radiation budget dataset. Bull Am Meteorol Soc 76:905–922

Wild M, Cechet R (2002) Downward longwave radiation in general circulation models: a case study at a semi-arid continental site. Tellus Ser A Dyn Meteorol Oceanogr 54:330–337

Willmott CJ, Robeson SM, Feddema JJ (1994) Estimating continental and terrestrial precipitation averages from rain-gauge networks. Int J Climatol 14:403–414